Correspondence to:
M. A. Bravo,
mbravo@dgeo.udec.cl

Ionospheric Response to Disturbed Winds During the 29 October 2003 Geomagnetic Storm in the Brazilian Sector

M.A. Bravo[1,2] (ID)**, I.S. Batista[1]** (ID)**, J.R. Souza[1], and A.J. Foppiano[2]** (ID)

[1]Instituto Nacional de Pesquisas Espaciais, INPE, São José dos Campos, Brazil, [2]Departamento de Geofísica, Universidad de Concepción, UdeC, Concepción, Chile

Abstract Modeling the ionosphere during disturbed periods is one of the most challenging tasks due to the complexity of the phenomena that affect the electric fields and the whole thermosphere environment. It is well known that both, prompt penetration electric fields and large amounts of energy deposited in the polar region during disturbed periods, produce significant disturbances in the global electron density distribution, in particular, in the equatorial ionization anomaly development. Besides, the disturbance dynamo, traveling atmospheric disturbances, and traveling ionospheric disturbances also affect the equatorial ionization anomaly density distribution. In this work we use the Sheffield University Plasmasphere-Ionosphere Model at Instituto Nacional de Pesquisas Espaciais, to simulate the drastic effects that were observed at the low-latitude ionosphere in the Brazilian region during a very intense magnetic storm event, the so-called 2003 Halloween storms. In the absence of measured vertical drift during the storm, a new vertical drift deduced from the interplanetary electric field combined with the time variation of the F region virtual height is used as input. The simulation results showed that, in the case of the disturbed thermospheric wind, the ionospheric observations are better explained when a novel traveling wave-like disturbance propagating from north to south, at a velocity equal to 300 m/s, is considered.

1. Introduction

In various investigation fields, physical models are used to describe the observed physical phenomena. The situation is not different when ionospheric physics is concerned. It is well known that the ionosphere can become globally disturbed by the space weather events that cause geomagnetic storms (e.g., Rishbeth, 1975; Prolss, 1977, among many others). These disturbances can severely interfere in the functioning of many technological devices such as those that relay on the Global Navigation Satellite System for navigation and positioning. For this reason, predicting the ionosphere behavior during such events is a very important task. There are many numerical models that are able to reproduce well the ionospheric conditions during quiet time. Among them we can list the following: LION (Bittencourt et al., 2007), SAMI2 (Huba et al., 2000), SUPIM (Bailey et al., 1993; Bailey & Sellek, 1990), and besides those found in Schunk (1996): GTIM, FLIP, TDIM, TIGCM, CTIM, CTIP, etc. In those models, time-dependent equations of continuity, momentum, and energy balance for the electrons and some ions along closed magnetic field lines are solved. However, when the ionosphere is modeled for disturbed geomagnetic conditions, the models do not always reproduce what the observations show.

Specifically, to model the equatorial and low-latitude ionosphere during disturbed periods, the ionospheric model should mainly consider the zonal electric field disturbances, the disturbed neutral winds, and probably traveling atmospheric disturbances (TADs) and/or traveling ionospheric disturbances (TIDs; see Abdu, 2005; Fuller-Rowell et al., 1994; Kelley, 2009; Prölss & Jung, 1978; Richmond & Matsushita, 1975; Rishbeth, 1975). In particular, it is necessary to consider the zonal electric field disturbances because they are prompt penetration electric fields and they are directly related to the vertical drift $\mathbf{E} \times \mathbf{B}$ that produces the plasma fountain effect, transporting plasma from equatorial to low latitudes, and developing the well-known equatorial ionization anomaly. The neutral disturbed composition would not be considered because they are only significant at middle and high latitudes. These disturbed parameters produce both positive and negative ionospheric storms, as well as phenomena such as equatorial counter-electrojet (Gouin, 1962), super plasma fountain (Balan et al., 2009; Tsurutani et al., 2004), and disturbance dynamo (Blanc & Richmond, 1980).

The SUPIM-INPE (Sheffield University Plasmasphere Ionosphere Model at Instituto Nacional de Pesquisas Espaciais [INPE]) is a modified version of SUPIM (Bailey & Balan, 1996) developed at the Aeronomy Division of the Atmospheric and Space Science Coordination of the National Institute for Space Research (INPE). In this modified version some input parameters, such as atmospheric neutral densities and solar EUV flux, were updated and the field line calculation was extended to lower altitudes in order to include the *E* region (Bravo et al., 2017; Santos et al., 2016; Souza et al., 2010, 2013). Some studies have demonstrated that this model reproduces well the ionosphere of equatorial, low, and middle latitudes during quiet conditions (Balan et al., 1995; Batista et al., 2011; Nogueira et al., 2013; Santos et al., 2017; Souza et al., 2013; Thampi et al., 2011) and at equatorial-low latitudes during geomagnetic storms (Abdu et al., 2013; Bravo et al., 2017; Santos et al., 2016).

An extreme geomagnetic storm, referred to in the literature as the Halloween Magnetic Storms, occurred in October–November 2003. There are many reports about this storm, and some of them also model its ionospheric effects. Such is the case of Batista et al. (2006), where they were able to reproduce the observations at the equator using SUPIM, including a proposed westward electric field disturbance just after the storm onset, which is in agreement with the same parameter measured by ROCSAT (Lin et al., 2005). However, in that study SUPIM was not able to reproduce the ionospheric effects observed after the storm commencement for low-latitude stations in the Brazilian region. The authors attributed the discrepancy between model results and observations, to a probable effect of a disturbed wind, but this hypothesis had not been tested until today. Moreover, Balan et al. (2009, 2010, 2013) have used a measured strong disturbed drift and an effective latitude-dependent equatorward wind (required for a super plasma fountain effect), the speed changing from 100 m/s at middle latitudes (~30° to 40°) to about zero at magnetic equator. However, such a disturbed wind pattern was not efficient to reproduce the observations during the Halloween storms over the Brazilian sector, and thus, a conjectured wave-like disturbance is needed to reproduce the ionospheric observations.

The main purpose of the present work is to investigate the role of some disturbed wind models in the ionospheric response to the first day of Halloween storms (29 October 2003), at equatorial and low latitudes over the Brazilian sector. A new disturbed wind model is proposed. It incorporates a wave-like disturbance wind. The equatorial ionospheric model of disturbed electric field from Bravo et al. (2017) is also used.

2. Data

The Halloween storms were produced by intense solar coronal mass ejections that followed the solar flares on 28 October 2003 at 11:10 UT (X-ray flux class X17) and on 29 October 2003 at 20:49 UT (X-ray flux class X10). The first coronal mass ejection reaches the Earth on 29 October 2003 at 06:11 UT (19 hr later) producing the first of the three geomagnetic storms and temporarily disabling and saturating some space instruments (Skoug et al., 2004). Figure 1 shows space parameters during the 28 to 31 October 2003 time interval (https://omniweb.gsfc.nasa.gov/). However, there are big gaps on the OMNIWeb data set of the interplanetary magnetic field vertical component (B_Z), the solar wind velocity (V_{SW}), and the interplanetary electric field (IEF), which is derived from B_Z and V_{SW}. To fill in these gaps of B_Z and V_{SW}, the ACE satellite data base is used (http://www.srl.caltech.edu/ACE/ASC/level2/lvl2DATA_MAG-SWEPAM.html). Unfortunately, although the B_Z filling-in is almost complete, the V_{SW} filling-in is rather limited. This is due to the saturation of the Solar Wind Electron Proton Alpha monitor of ACE satellite. Note that no determination of IEF is readily accessible for 31 October 2003 between 01:30 and 11:30 UT, although B_Z and V_{SW} are available. The filling-in data are out of phase by 40 min with respect to the OMNIWeb data. This is taking into account when plotted as the green line in Figure 1. Figure 1 also shows the ground-based indices *Dst* (http://wdc.kugi.kyoto-u.ac.jp) and *AE* (https://omniweb.gsfc.nasa.gov/).

From Figure 1 it is clear that when B_Z exhibits the largest fluctuations after the storm sudden commencement on 29 October 2003, the final *Dst* shows the development of the first two storms (main phase and recovery of the first and the most of the main phase of the second). *Dst* shows a relative minimum of −151 nT at 10 UT. During the same interval concurrent fluctuations are observed in *AE*.

The diurnal variation of the *F* layer critical frequency (*foF*2) and peak height (*hmF*2) used in the present work is from ionospheric stations of the South American region and its vicinity. They are listed in Table 1, and their relative locations are shown in the Figure 2a.
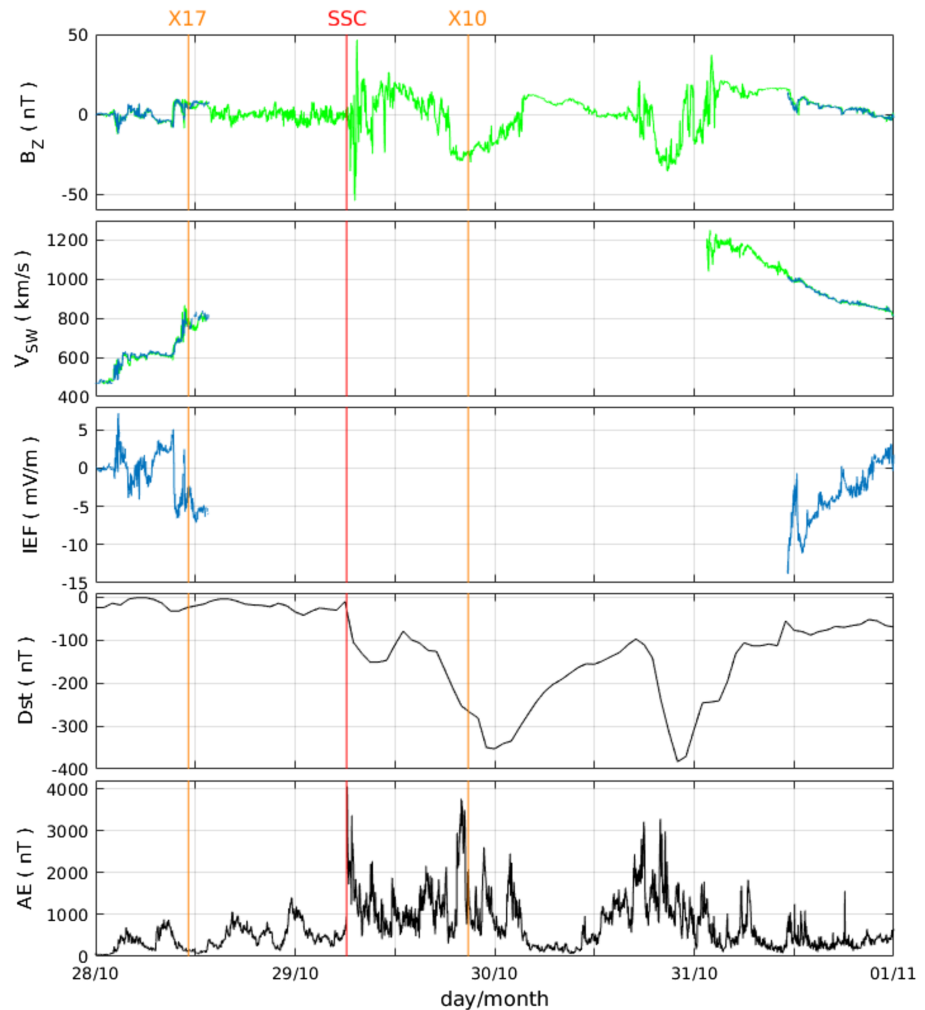
Figure 1. Space and ground-based parameters for 28–31 October 2003. From top, interplanetary magnetic field vertical component (B_Z), solar wind velocity (V_{SW}), interplanetary electric field (*IEF*), disturbance storm time index (*Dst*), and Auroral electrojet index (*AE*). Space parameters from OMNIWeb data (blue) and filled-in values from the ACE satellite (green). Ground parameters *Dst* from WDC, Kyoto and *AE* from OMNIWeb data.

Figure 2b gives the indicated diurnal variations for 29 October 2003. Reference diurnal variations for geomagnetic quiet day 11 October 2003 ($Ap = 2$) are also shown for all stations except RA (18.5°N, 68.0°W). In the case of RA, quiet day 29 September 2003 ($Ap = 4$) is used instead, because there were no observations for 11 October 2003. Note also that $h'F$ is used for Concepción instead of $hmF2$.

It is evident that there are clear perturbations in $foF2$ and $hmF2$ during the disturbed day with reference to the quiet day for several stations. In some cases, similar disturbances seem to occur in more than one location. For example, the oscillation in $foF2$ with a peak at 10 UT (horizontal red arrow) and subsequent decrease with a minimum around 12 UT (vertical black arrow) occurs almost simultaneously over CP and TU. In the same way, the marked lowering of $hmF2$ between 10 and 12 UT and subsequent elevation of the layer also seems to occur simultaneously over CP and TU, considering that these two stations are well separated (~20° of geographic longitude and ~4° of geographic latitude). CO and AI stations also show the peak in $foF2$ at 09–10 UT, but with smaller amplitude than those at CP and TU. On the other hand, the observations of $hmF2$ in CO and AI do not show clear similarities. Almost simultaneous disturbed effects in $foF2$ and $hmF2$ are also observed between 09 and 12 UT in SL and FZ. In this case the similarities could be attributed to the proximity between the two stations (differences of only ~1.3° of geographic latitudes and ~4.7° of magnetic latitude apart from each other).

In the present work only the first day of the 29 October 2003 storm will be analyzed.

Table 1
List of Stations Used in the Present Work Ordered According the Geographic Latitude

Station	Geographic latitude	Geographic longitude	Local time	Geomagnetic latitude	Geomagnetic longitude	Magnetic declination
Ramey (RA)	18.5°	292.0°	UT-5	28.6°	8.1°	−11.6°
São Luís (SL)	−2.5°	315.8°	UT-3	−1.6°	27.4°	−20.8°
Fortaleza (FZ)	−3.8°	322.0°	UT-3	−6.1°	32.5°	−21.5°
Ascencion Island (AI)	−7.9°	346.0°	UT-1	−18.6°	55.4°	−16.6°
Jicamarca (JI)	−12.0°	283.2°	UT-5	0.5°	355.2°	0.0°
Cachoeira Paulista (CP)	−22.7°	315.0°	UT-3	−17.7°	21.1°	−20.8°
Tucumán (TU)	−26.9°	294.6°	UT-4	−14.5°	4.7°	−4.3°
Concepción (CO)	−36.8°	287.0°	UT-5	−23.2°	359.3°	7.4°
Port Stanley (PS)	−51.6°	302.1°	UT-4	−38.2°	10.6°	3.7°

Note. The geomagnetic coordinates are obtained from IGRF-12 for the year 2003 at the Earth's surface (http://www.geo-mag.bgs.ac.uk/data_service/models_compass/coord_calc.html). IGRF = International Geomagnetic Reference Field.

3. Models

In order to model the above-described variations of *foF*2 and *hmF*2, we have used the SUPIM-INPE model version. As already used in Bravo et al. (2017), the SUPIM solves the coupled time-dependent equations of continuity, momentum, and energy balance for the ions (O^+, H^+, He^+, N_2^+, NO^+, and O_2^+) and electrons along closed magnetic field lines. The SUPIM-INPE extends the calculations along the magnetic field lines from its original lower apex and base altitude limits from 150 and 130 km (Bailey et al., 1993; Bailey & Balan, 1996) down to 90 and 80 km, respectively, and adds the calculations for a seventh ion N^+ (Souza et al., 2010, 2013). Moreover, the chemical reaction scheme from Huba et al. (2000), which is prepared to include E region, has been used. The photochemical equilibrium condition was applied only at the base altitudes as also used by original SUPIM.

The model uses as main input parameters the EUV flux, the neutral densities, the zonal electric field (or in this case the $\mathbf{E} \times \mathbf{B}$ drift) and the neutral wind. The EUV flux used is obtained from EUVAC model (Richards et al., 1994) except for the X-ray and Lyman-α fluxes which are taken from the SOLAR2000 model (Tobiska et al., 2000). Both ionizing solar radiation are mean values and representative of noon time. In the model, the diurnal variation has been calculated using the solar zenith angle. The neutral densities are from NRLMSISE-00 (Picone et al., 2002). In particular, to simulate the low and equatorial latitude ionosphere using SUPIM-INPE model, it is necessary to know the disturbed $\mathbf{E} \times \mathbf{B}$ drift and disturbed neutral winds, which were not measured during the event at the region under study. Here, we propose new disturbed vertical drift and disturbed neutral wind models to well represent the disturbed ionospheric conditions for this storm.

The SUPIM-INPE provides as output the vertical profiles for the ions and electrons, which can be used to calculate the ionospheric parameters *foF*2 and *hmF*2.

3.1. Disturbed E × B Drift Inferred From IEF and d*h'F*/d*t*

In the here proposed model, the disturbed vertical drift is assumed to be the composite of two parts, as previously suggested by Bravo et al. (2017) to model some magnetically disturbed conditions.

The first one, covering the initial phase of the storm, is the sum of a disturbed drift derived from IEF and the quiet time equatorial latitude model of Scherliess and Fejer (1999). This methodology closely follows the Kelley and Retterer (2008) work. It consists of considering IEF efficiencies of 10% when the B_Z points to south (negative) and of 3% when B_Z points to north (positive), superposed to the preexisting field of quiet conditions. Specifically,

$$V_Z = \text{disturbed drift} + \text{quiet drift} = (Eff \times \text{IEF}) + (Scherliess \& Fejer, 1999) \tag{1}$$

where the efficiency *Eff* = 0.1 for B_Z negative and *Eff* = 0.03 for B_Z positive.

Note that in our case a further reduction of the efficiencies to 5% after 18 UT is made. The IEF is calculated according to the expression: $\text{IEF (mV/m)} = -V_{SW} \text{(km/s)} \times B_Z \text{(nT; GSM)} \times 10^{-3}$ (OMNIWeb). In the absence
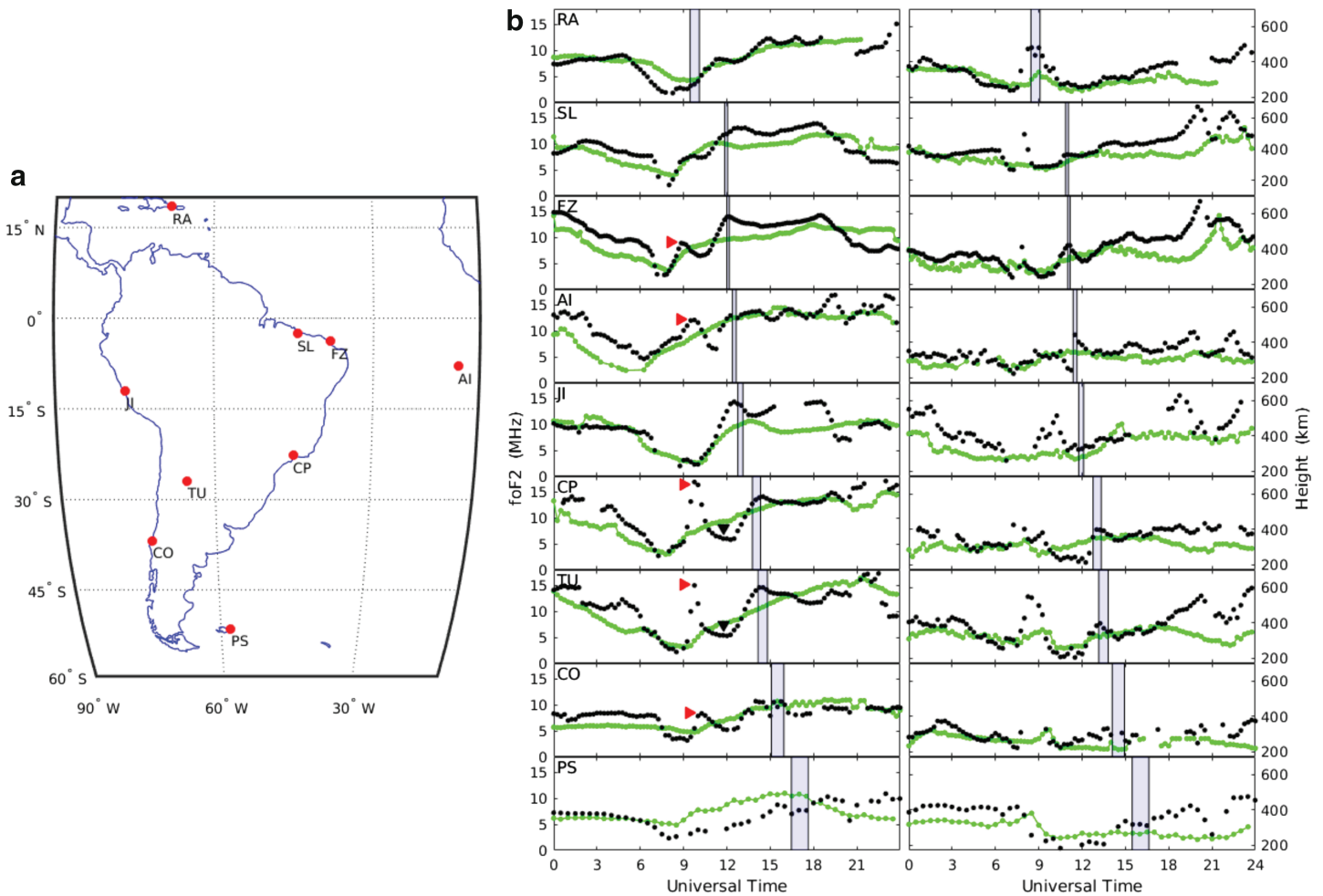
Figure 2. (a) Location of the digisonde/ionosonde stations used in the present work. Dashed line indicates the magnetic equator. (b). Observed F layer critical frequency, $foF2$ (left) and peak height, $hmF2$ ($h'F2$ for Concepción; CO; 36.8°S, 73.0°W; right) during the storm day, 29 October 2003 (black dots), and during a quiet day (green dots): 11 October 2003 for all stations; 29 September 2003 for Ramey (RA; 18.5°N, 68.0°W). Vertical lines and shadow intervals are explained in the text.

of V_{SW} data, we have used a mean solar wind velocity of 1,000 km/s (average between the values at the limits of the gap, 800 and 1,200 km/s; Figure 1), which is consistent with wind values for others intense storms.

The second part, corresponding to the prereversal enhancement time interval, is derived from time variation of the F region height (d$h'F$/dt). d$h'F$/dt is calculated from the mean virtual height of reflection for 4, 5, and 6 MHz signals observed from ionograms when the mean heights only are higher than 290 km. That is,

$$V_Z = \frac{1}{3}\left(\frac{\Delta h'_{4MHz}}{\Delta t} + \frac{\Delta h'_{5MHz}}{\Delta t} + \frac{\Delta h'_{6MHz}}{\Delta t}\right) \qquad (2)$$

This procedure was also used by Batista et al. (2006), because, for this height range, d$h'F$/dt mostly depends on the vertical drift velocities since the chemical recombination processes at this height range are less significant (Bittencourt & Abdu, 1981).

The total disturbed $\mathbf{E} \times \mathbf{B}$ drift at approximately the magnetic equator (SL, 2.5°S, 315.8°E) for 29 October 2003, with the above-described modifications, is shown in Figure 3.

3.2. Disturbed Wind Calculations

In the present proposed model the disturbed wind is assumed to be the sum of two components. The first component is a quiet time wind calculated using the Horizontal Wind Model 1993, HWM93 (Hedin et al.,
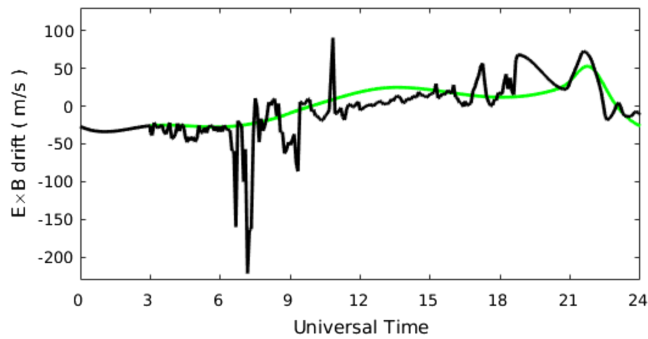
Figure 3. E × B drift for São Luís (2.5°S, 44.2°W) during 29 October 2003. Black line model disturbed vertical drift. Green line quiet time vertical drift.
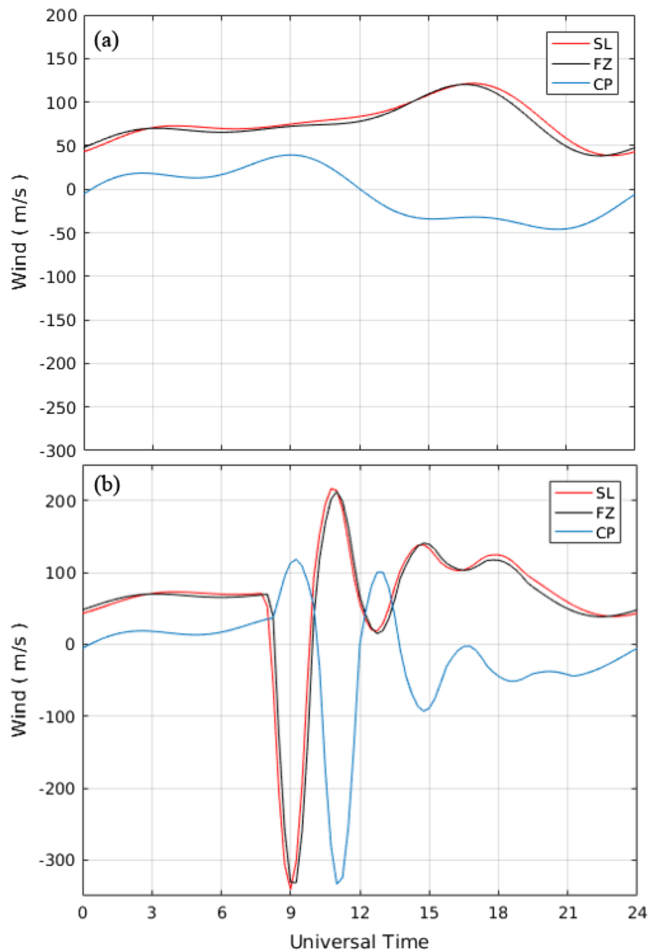

Figure 4. Proposed model the disturbed wind at 250-km height. (a) Quiet time wind calculated using the Horizontal Wind Model 1993 at Sao Luis (SL; 2.5°S, 44.2°W), Fortaleza (FZ; 3.8°S, 38.0°W), and Cachoeira Paulista (CP; 22.7°S, 45.0°W). (b) Transequatorial wave-like perturbation for the same three stations. The wave-like perturbation amplitudes are −450, +150, −75, +38, −19, and +10 m/s because these include the amplitude of the Horizontal Wind Model 1993 wind.

1996). The diurnal variation of this wind (29 October 2003) is shown in Figure 4a for three Brazilian stations and the latitude height distribution of the wind on Figure 5, along the Cachoeira Paulista magnetic meridian (~21°E). The second component is a transequatorial wave-like perturbation assumed to be propagating from north to south. This perturbation is thought to originate at the north auroral zone as energy is deposited into the thermosphere at the start of the storm. The model seems to be reasonable since it is consistent with ample evidence of propagating-like features in the diurnal variations of both $foF2$ and $hmF2$ (Abdu, 2005; Batista et al., 2006, 2012; Fuller-Rowell et al., 1994; Kelley, 2009; Prölss & Jung, 1978; Richmond & Matsushita, 1975; Rishbeth, 1975). Here it is assumed that the perturbation front is parallel to geographic latitudes and that is moves along a geographic meridian. Careful considerations of the quasi-oscillations of $foF2$ and $hmF2$ (section 2; Figure 2b) suggest that the wave-like perturbation's wave length is about 2,000 km, the propagation speed of around 300 m/s at some 250-km height. The vertical lines in Figure 2b indicate when the perturbation reached the different stations, assuming that it is visible on $hmF2$ over FZ between 11:00 and 11:10 UT and perturbs $foF2$ between 12:00 and 12:10 UT. The separation between the vertical lines indicates the range of propagation speeds being 300 m/s ± 10%.

The wave-like perturbation is assumed to attenuate with time, in accordance with the modeling results of Richmond and Matsushita (1975), which simulated the winds and temperature variations in the thermosphere during a large magnetic substorm. Specific amplitudes for various semiperiods are for a sinusoidal curve with a first trough of amplitude of −450 m/s (negative is south) in the first semiperiod, then it is followed by a crest of amplitude +150 m/s (positive is north) in the second semiperiod. The amplitudes of the following semiperiods were −75, +38, −19, and +10 m/s, respectively.

The estimations of wave length, propagation speed, and amplitudes were reached after several iterations, changing one parameter at the time, using $foF2$ and $hmF2$ variations over FZ and CP. For example, a 25% change of the first trough amplitude resulted in a change of 8% in $foF2$ and 5% in $hmF2$.

The perturbation wave form as it reaches three stations is shown in Figure 4b. The latitude height variation of the full disturbed wind model is shown in Figure 6, also along the Cachoeira Paulista magnetic meridian (~21°E).

It is important to note in Figures 4b and 6 that an additional positive disturbance (northward) of 75-m/s amplitude was placed between 08:30 and 10:30 UT which was necessary to reproduce the $foF2$ peak at 10 UT in CP.

4. Results

The SUPIM-INPE simulation results using the disturbed E × B drift and quiet wind and the disturbed E × B drift and the disturbed wind, during the 29 October 2003, are shown for SL and FZ (near equatorial latitudes) and CP (low latitude) in Figures 7, 8, and 9, respectively. The figures show the $foF2$ and $hmF2$ simulations and observations together with the Dst and Kp indices.
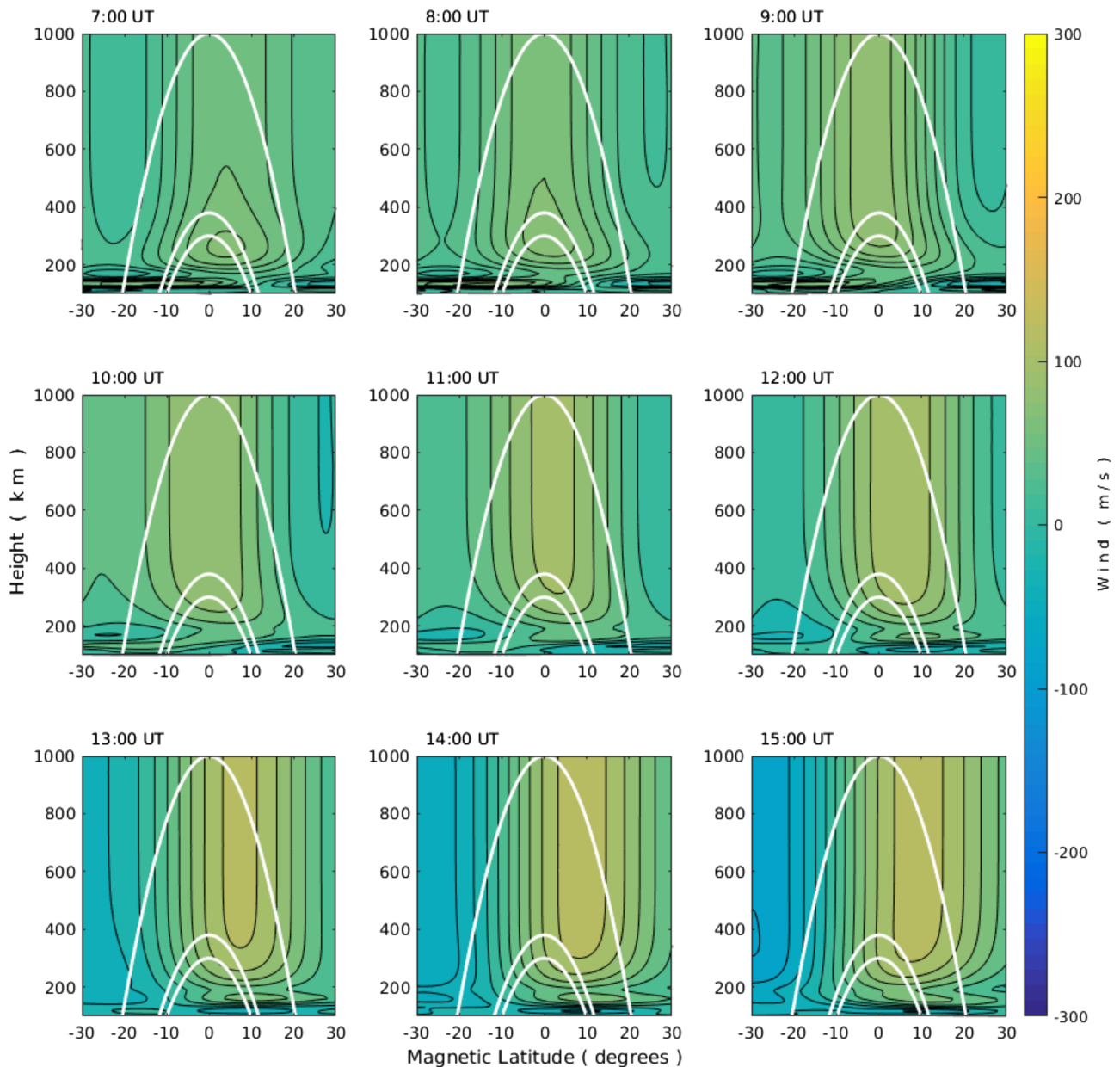
Figure 5. Horizontal Wind Model 1993 wind distributions along the ~21°E magnetic meridian (the Cachoeira Paulista magnetic meridian) during geomagnetic quiet conditions. White lines are the magnetic field lines that intercept the latitudes of Cachoeira Paulista (22.7°S, 45.0°W), Fortaleza (3.8°S, 38.0°W), and Sao Luis (2.5°S, 44.2°W) at 300-km height.

4.1. Results Using Disturbed E × B Drift and Quiet Wind

Although IEF calculations were made with a constant solar wind speed, the simulations for SL (Figure 7), using the disturbed vertical drift (IEF plus d$h'F$/dt) reproduce well the $hmF2$ observations from the beginning of the storm (~06 UT) until 22 UT. For $foF2$ the simulations agree with the observations from ~6 to 9 UT and after 18 UT. Before the beginning of the storm, the agreement is not so good for both $foF2$ and $hmF2$. However, we must keep in mind that the drift used for this time interval is that of the quiet time as given by the empirical model (Scherliess & Fejer, 1999). Moreover, spread F is prevalent during 00–04 UT; thus, the real $foF2$ is likely to be smaller and $hmF2$ larger than indicated in the figure. In addition, the ionospheric conditions of the previous days (26–28 October 2003) are not quiet (see Blagoveshchensky et al., 2006).
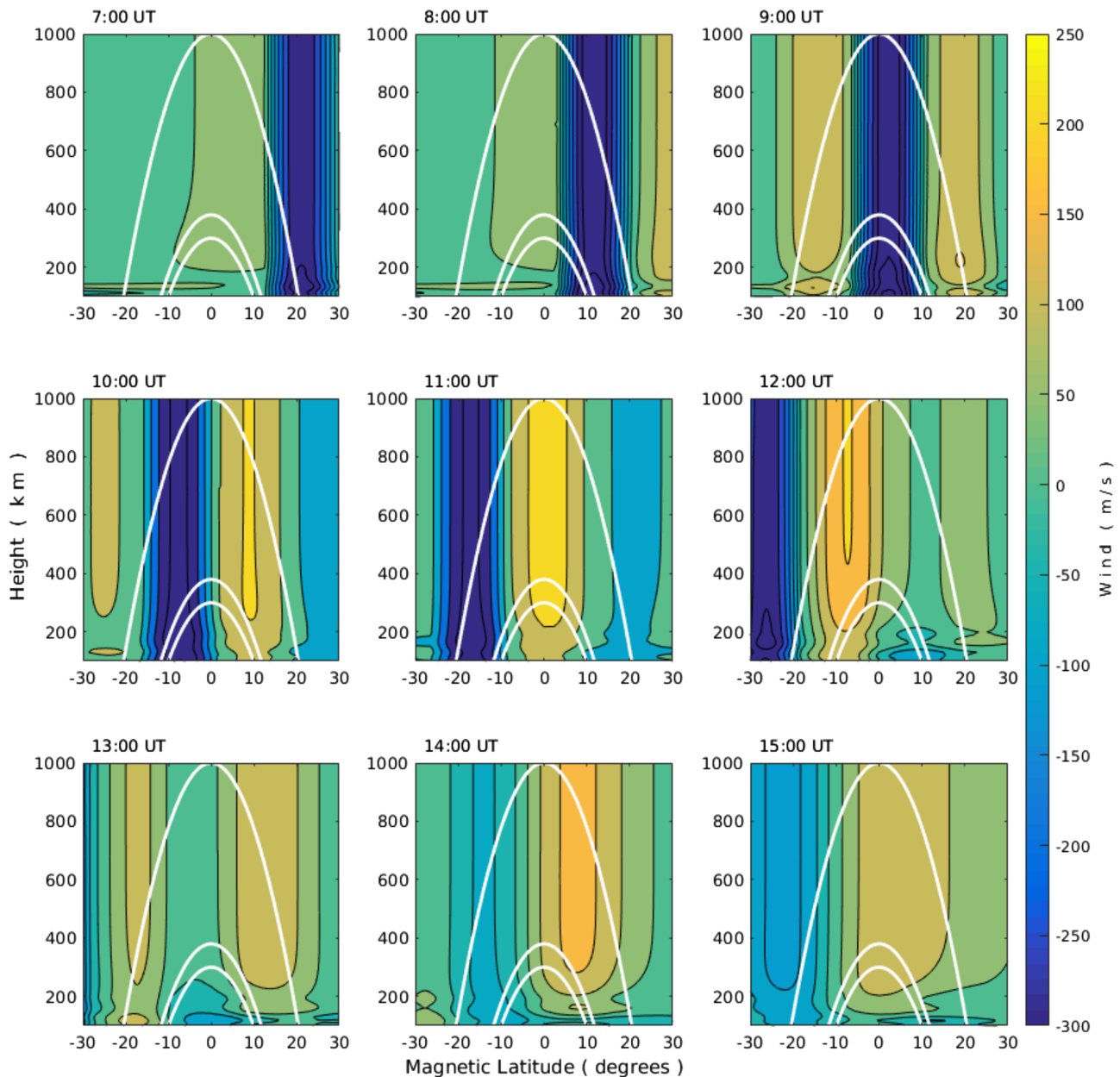
Figure 6. Disturbed wind model distributions along the ~21°E magnetic meridian (the Cachoeira Paulista magnetic meridian) during geomagnetic disturbed conditions. White lines are the magnetic field lines that intercept the latitudes of Cachoeira Paulista (22.7°S, 45.0°W), Fortaleza (3.8°S, 38.0°W), and Sao Luis (2.5°S, 44.2°W) at 300-km height.

The agreement between simulations and observations for FZ (Figure 8) is better for *foF2* and almost as good for *hmF2* as already discussed at SL.

In the case of CP (Figure 9), the low-latitude station, the agreement between simulation and observation is not so good as for SL and FZ, the near equatorial stations. For *foF2* the agreement is only good in 07- to 09 and 20- to 24-UT intervals and for *hmF2* is for 00- to 09- and 19- to 22-UT intervals. This is because while the equatorial ionosphere is mainly affected by the vertical drift, for the low-latitude ionosphere the effect of the neutral wind is as important as or even more important than the $\mathbf{E} \times \mathbf{B}$ drift effect. The simulations for CP show large differences from the observations for both *foF2* and *hmF2* mainly because a quiet time neutral wind model was used.
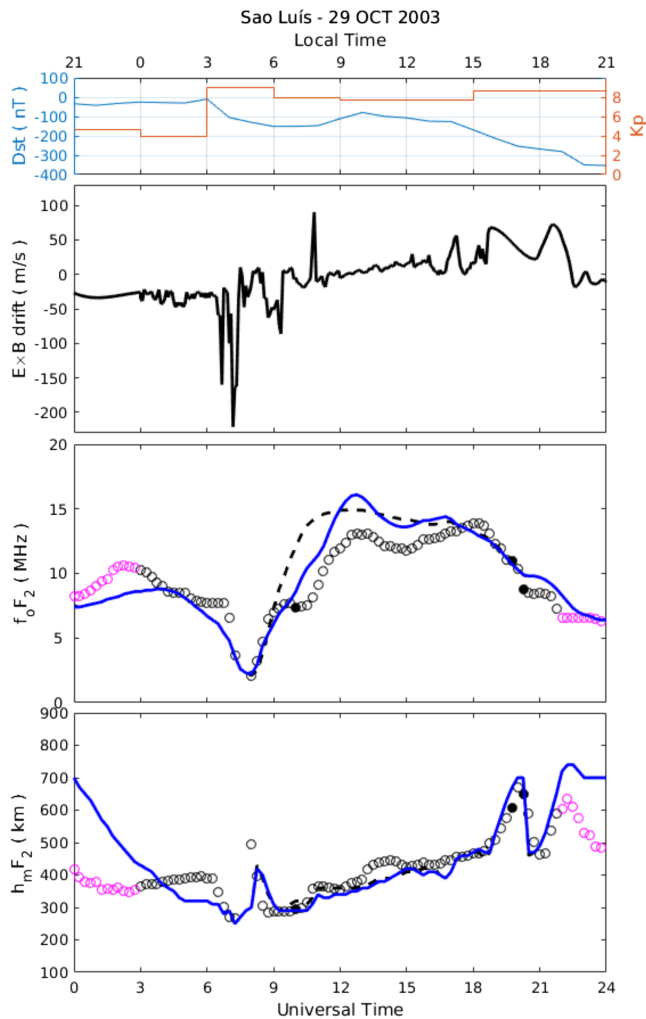
Figure 7. Simulated (lines) and observed (circles) *foF*2 and *hmF*2 over São Luís (2.5°S, 44.2°W) for 29 October 2003. (first panel) *Dst* and *Kp* indices. (second panel) Vertical drift derived from *IEF*-d*h'F*/d*t*. (third panel) *foF*2 and (fourth panel) *hmF*2. (dashed black line) Simulation with quiet time wind model (HWM93). (blue line) Simulation with disturbed wind model. (filled-in circles) *F*3 layer presence. (magenta circles) Spread *F* occurrence.

4.2. Results Using Disturbed E × B Drift and Disturbed Wind

It is quite clear that the agreement between simulations and observations for SL, FZ, and CP improved considerably when using the disturbance wind model.

When the results for SL and FZ are considered (Figures 7 and 8), we can observe, as expected, no significant difference between modeled results and observations when the disturbed wind is considered in relation to the results using the quiet time wind model. As explained before, this is due to the dominance of the effect of the **E × B** term at equatorial latitudes.

In the case of CP (Figure 9), the *foF*2-simulation reproduced the large peak at 10 UT, the subsequent decrease between 10 and 13 UT, and partially the subsequent wave behavior after 13 UT. In the same way, the *hmF*2 simulations reproduced the anomalous decrease between 09 and 12 UT and partially the subsequent wave behavior after 12 UT.

It is to be noted that a disturbance neutral wind at the equator has larger effect in *foF*2 than in *hmF*2, while the same wind affects both *foF*2 and *hmF*2 over CP.

The electron density distribution as a function of latitude and altitude, along the magnetic meridian affected by the traveling wave-like disturbance is presented in Figure 10. This figure shows the evolution of a disturbed equatorial ionization anomaly at each hour between 7 and 18 UT, during 29 October. At ~09 UT, the disturbed wind produced a peak in *F*2 layer density close to the latitude of FZ. This peak moved southward reaching the latitude of CP approximately 1 hr later, and in the next 2 hr it reached −30° latitude. Between 14 and 16 UT the disturbed latitudinal distribution of the ionization shows three peaks. From 17 UT the distribution returns to its normal behavior due to the lower wind amplitudes.

5. Discussion

Present results are only for stations within the equatorial and low-latitude range in the Brazilian sector. The magnetic declinations in these three stations are almost the same. The angle between the thermospheric wind and effective wind meridian components is again very close (meridional effective wind = (U$_M$ cos(D) - U$_Z$ sin(D))*sin I; with U$_M$: meridional wind, U$_Z$: zonal wind, D: declination, I: inclination). This means that whether the perturbation wind front is circular (point source in the North Hemisphere) or parallel to geographic latitude (extended source), the effect of the wind will be similar at all three stations. Furthermore, for all three stations the diurnal variation epoch considered here is the same, thus avoiding further considerations needed to be made relative to the thermospheric wind effect in the continuity equation. However, there are other important considerations to be made. Although a fixed wavelength and perturbation speed have been assumed, it is likely that both depend on latitude. These may explain some of the differences in the shape of the quasiperiodic oscillations of the diurnal variations of *foF*2 and *hmF*2 for various stations. Thus, no resort to other processes may be needed.

In particular, a small increase in *hmF*2 is observed at PS at about 18:00 UT (Figure 2b). This is some two 2 hr the calculated arrival of the perturbation assuming a 300-m/s speed. However, if the perturbation speed decreases to about 210 m/s with increasing latitude, the small *hmF*2 increase mentioned is well explained. Furthermore, although there are few observations at CO after the calculated arrival of the perturbation, these observations are also consistent with a propagation speed of assumed 200 m/s.

It is true that no *hmF*2 increase is observed at JI at the time of the perturbation arrival (Figure 2b). However, for this station the sunrise terminator takes place only within an hour of the perturbation arrival time.
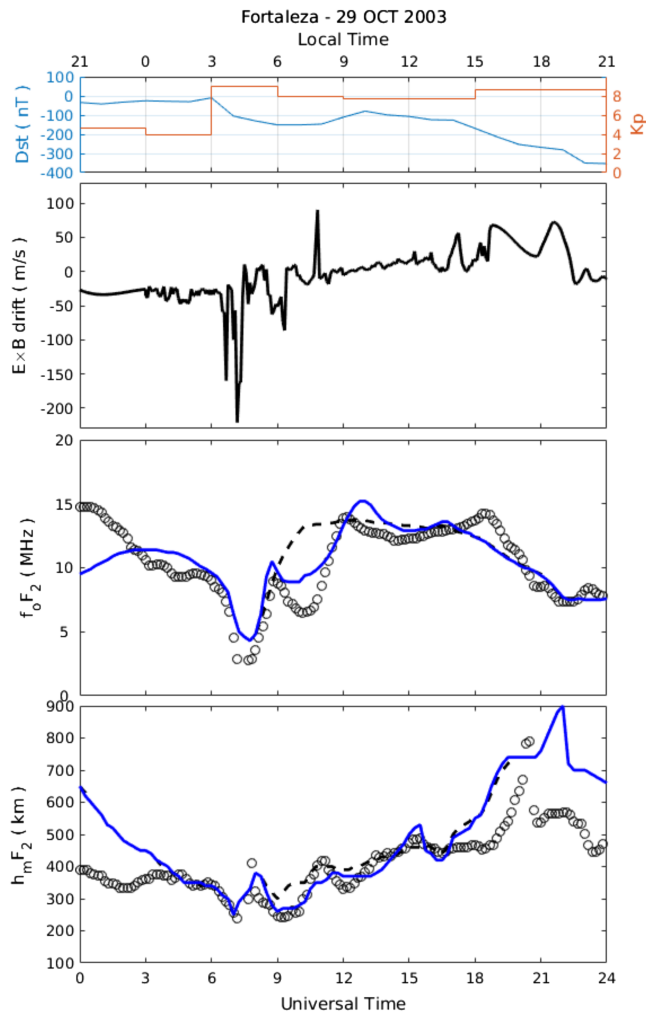
Figure 8. Simulated (lines) and observed (circles) *foF*2 and *hmF*2 over Fortaleza (3.8°S, 38.0°W) for 29 October 2003. (first panel) *Dst* and *Kp* indices. (second panel) Vertical drift derived from *IEF*-d*h′F*/d*t*. (third panel) *foF*2 and (fourth panel) *hmF*2. (dashed black line) Simulation with quiet time wind model (HWM93). (blue line) Simulation with disturbed wind model. (filled-in circles) *F*3 layer presence. (magenta circles) Spread *F* occurrence.

Moreover, at SL, the other equatorial station, a small *hmF*2 increase can be observed. There, the perturbation arrival does coincide with the sunrise terminator. Since for the two stations no *hmF*2 increases are expected, the terminator and perturbation effects may be compounded.

According to Bravo et al. (2017), in the absence of vertical drift measurements from incoherent scatter radar to be used as input parameters for ionospheric models, the best options are to use the vertical drift average for 150 km height from the Jicamarca Unattended Long-Term studies of the Ionosphere and Atmosphere radar (see Chau & Woodman, 2004) or the vertical drift deduced from magnetometers (see Anderson et al., 2002, 2004, 2006), both used for daytime (06–18 LT) and combined with d*h′F*/d*t* from ionosondes for the prereversal enhancement hours and after the sunset (18–24 LT). However, for the case analyzed in the present study, the ionospheric disturbance that occurred on 29 October 2003, these measurements were not available for the Brazilian longitude sector. Besides, they are not the best options when the geomagnetic storm starts during the nighttime hours as is the case for the 29 October 2003 in the Brazilian region. For this reason we have used the vertical drift derived from IEF according to the method proposed by Kelley and Retterer (2008). According to the literature, efficiencies can vary between 3% and 14% depending on the direction of B_Z component of the IMF and the local time (e.g., Burke et al., 2007; Denardini et al., 2011; Huang et al., 2007, 2010; Kelley et al., 2003; Wei et al., 2008). We have used the efficiencies of Kelley and Retterer (2008), that is, 10% for southward B_Z and 3% for northward B_Z, except at 19–20 UT (16–17 LT, Figure 3), for which we have used 5%.

The drift obtained (Figure 3) is in agreement with the ROCSAT-1 satellite data presented in Lin et al. (2005), which correspond to $\mathbf{E} \times \mathbf{B}$ drift each 97 min at 300-km height, for the magnetic equator and 70°W geographical longitude during 29 October 2003. There is coherence, for example, in the minimum at the beginning of the storm (~06 UT) and the maximum in the evening (18–21 UT). However, this drift could not be used in our simulations due to its low frequency of sampling (each 97 min).

Also, the drift used in the present work is in agreement with the drift used by Batista et al. (2006) at the beginning of the storm between 06 and 08 UT. Both drifts have a decrement between 07 and 08 UT that reproduces the observations in *foF*2 and *hmF*2 in SL, FZ, and CP. However, after 09 UT the simulations in Batista et al. (2006) are not able to reproduce the observations. Originally, some tests with modifications in the drift model from Batista et al. (2006), inserting a positive peak after its decrease with the same amplitude, were used for the SUPIM simulations, in order to simulate an overshielding condition after an undershielding event. The simulation results using this drift (not shown here) were able to reproduce the *foF*2 observations between 09 and 12 UT in SL and FZ, but not in CP, while the results for *hmF*2 did not agree with the observations at none of the three stations. On the other hand, simulations using a disturbed wind similar to the wind used in Balan et al. (2009, 2010), that is, a wind that has zero amplitude at the magnetic equator and amplitude near to 100 m/s at middle latitudes (± 20°), have been ineffective to reproduce the observations during the Halloween storm over the Brazilian sector. The results using Balan's disturbed winds at the Brazilian sector showed no significant effects compared to no wind. Another disturbed wind configuration was necessary. One possibility was asymmetric neutral winds which can do asymmetric positive storms with respect to the equator (Balan et al., 2013) and considering that the TADs could be a good option.

The latitude height plasma-frequency distribution simulations presented in Figure 10 are consistent with the total electron content (TEC) observation maps over Brazilian sector from Batista et al. (2006), Figure 4. In
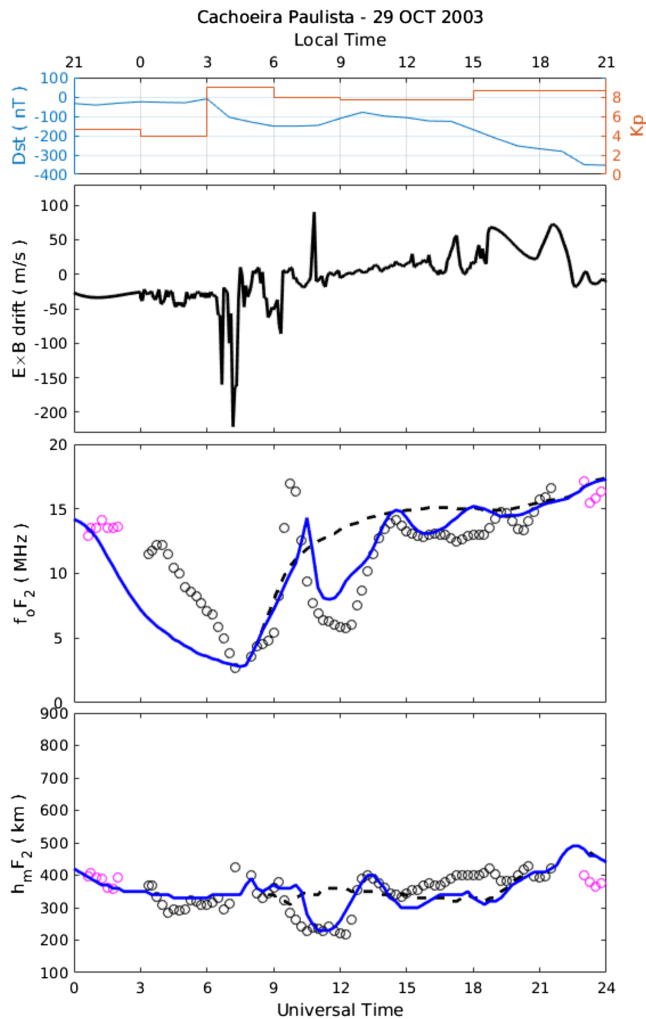
Figure 9. Simulated (lines) and observed (circles) *foF*2 and *hmF*2 over Cachoeira Paulista (22.7°S, 45.0°W) for 29 October 2003. (first panel) *Dst* and *Kp* indices. (second panel) Vertical drift derived from *IEF*-d*h′F/dt*. (third panel) *foF*2 and (fourth panel) *hmF*2. (dashed black line) Simulation with quiet time wind model (Horizontal Wind Model 1993). (blue line) Simulation with disturbed wind model. (filled-in circles) *F*3 layer presence. (magenta circles) Spread *F* occurrence.

their figure, the quiet time TEC is observed between 07 and 08 UT (04–05 LT) of the disturbed day 29 October 2003 and is similar to the characteristics of the quiet time TEC (11 October 2003). This is in agreement with the very low plasma frequency simulations shown in Figure 10 (electron density is proportional to the square of plasma frequency). The following increase in TEC observed near FZ and SL but not in CP between 08 and 09 UT (their Figure 4) is consistent with what is shown in Figure 10, 09 UT. Later on (09–10 UT) there is a strong peak of TEC over CP that seems to move southward in the following hours (10–11 UT), which also agrees with the electron density simulation shown in Figure 10 between 10 and 12 UT. The wind configuration having a wave-like propagating southward (interhemispheric propagation) seems to be responsible for the great peak in *foF*2 over CP at 10 UT. Batista et al. (2012) shows similar early morning enhancement in *foF*2 over CP during the 24 November 2001 and 31 March 2001 storms. For the 24 November 2001, Batista et al. (2012) deduced meridional winds with drastic and sharp wind inversions, compatible with the hypothesis of surges in the wind and also compatible with the wave like used in the present work.

Analysis of disturbances in the TEC maps for the European sector during the 29 October 2003 (Borries et al., 2009) gives a propagation speed equal to 976 ± 201 m/s and a period equal to 56 ± 11 min. This is 3 times larger than the propagation speed used in the present work. On the other hand, if we consider that the perturbation observed in RA at 08 UT was produced by the wave passing through that location, we can calculate a propagation speed equal to ~750 m/s, value which is closer to that found in Borries et al. (2009). Most time lags between the increase of *AE* index and the subsequent increase in *foF*2 are of the order of 1.5 to 3.5 hr (Prölss & Jung, 1978). Thus, if we consider that the storm started at 06:10 UT, it would be possible to observe effects at 08 UT in RA. Our propagation speed (300 m/s) could be due to a decline in speed, as it advances in latitude as suggested in the simulations presented in Richmond and Matsushita (1975) as well as in the work of Shiokawa et al. (2007) for the magnetic storm of 31 March 2001. In general, the propagation velocity of TADs could be of the order of 400 to 1,100 m/s (Richmond & Matsushita, 1975), but on the other hand, the TID that is the signature in the ionosphere of the passage of the TAD could have different speeds and significant variations with height (Balthazor & Moffett, 1997) not considered here.

The positive disturbance (northward) that was introduced in the wave-like wind velocity for CP (Figure 6, bottom panel) in order to reproduce the *foF*2 peak at 10 UT could be explained as the combined effect of conjugate TADs originated in both north and south auroral zones, which interfere constructively, increasing the magnitude of the TID in a way similar to that seen in the simulation of Balthazor and Moffett (1997).

Chen et al. (2016) studied the variations of nighttime *hmF*2 over the American sector during the 28–29 October 2003 storm period, using the National Center for Atmospheric Research Thermosphere-Ionosphere Electrodynamics Global Circulation Model. Their numerical experiments, in comparison with the data of Dyess (32.4°N, 99.8°W), Eglin (30.5°N, 86.5°W), Ramey (18.5°N, 67.1°W), and Jicamarca (12.0°S, 76.8°W) ionosonde stations, suggest that the nighttime increase of *hmF*2 at 07–10 UT of 29 October (see Ramey and Jicamarca in Figure 2a) is mainly caused by TADs from the high latitudes of the Northern Hemisphere. This equatorialward wind (from north) would have speeds larger than 200 m/s, agreeing with our wind. Their simulations show equatorward winds traveling from the north as well as from the south. The equatorward wind propagating from south could explain the additional disturbance (northward) placed between 08:30 and 10:30 UT necessary to reproduce the *foF*2 peak at 10 UT in CP. However,
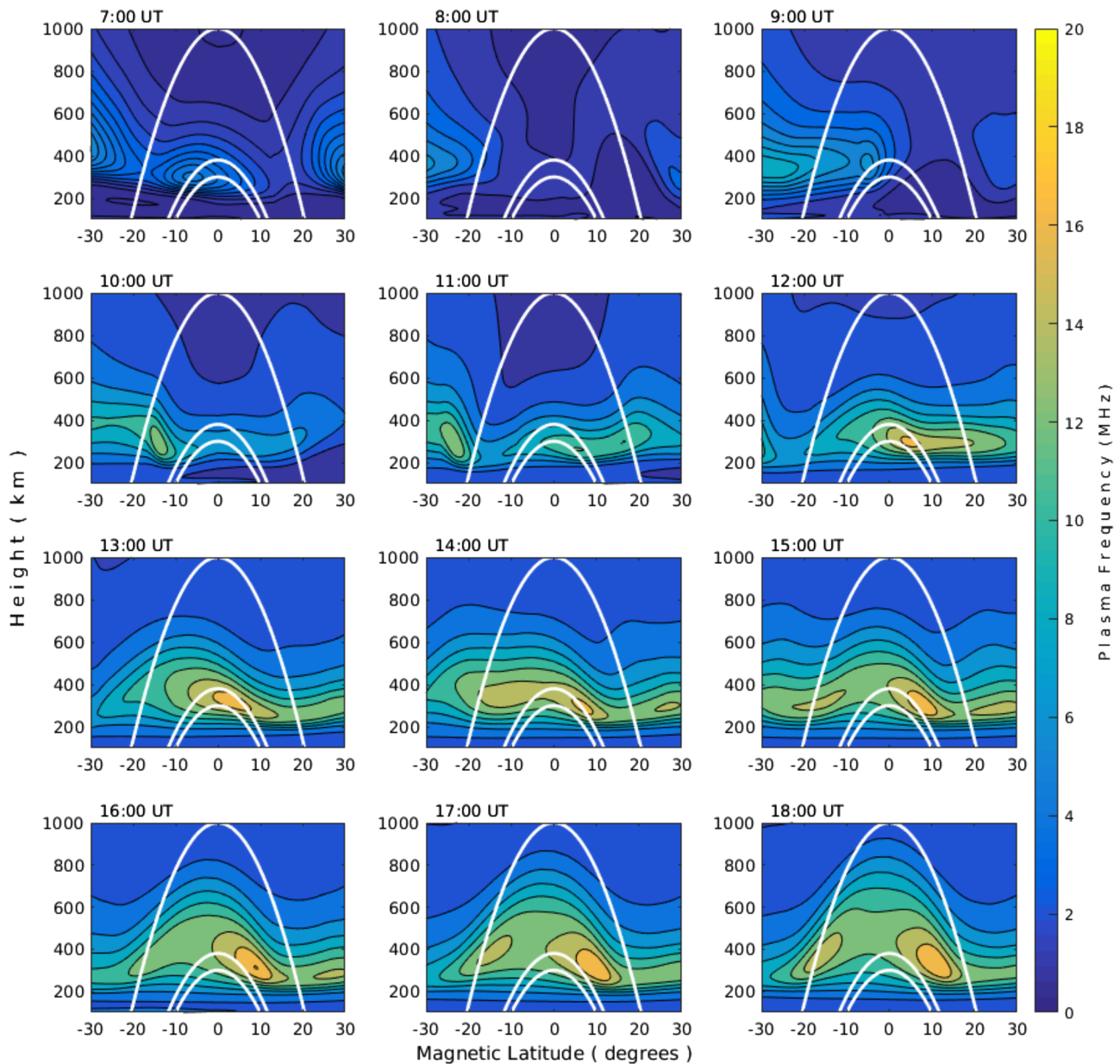
Figure 10. The Sheffield University Plasmasphere Ionosphere Model at Instituto Nacional de Pesquisas Espaciais simulated plasma frequency distribution along the ~21°E magnetic meridian (Cachoeira Paulista magnetic meridian) affected by the traveling wave-like disturbance propagating from north to south during 29 October 2003. White lines are the magnetic field lines that intercept the latitudes of Cachoeira Paulista (22.7°S, 45.0°W), Fortaleza (3.8°S, 38.0°W), and Sao Luis (2.5°S, 44.2°W) at 300-km height.

they show a dominant transequatorial wind from the south (which is contrary to ours), but this wind should lower the layer in the Northern Hemisphere, which is not seen in RA (Figure 2a). On the other hand, analysis of TEC maps over North America during 29–30 October 2003 presented in Ding et al. (2007) showed the existence of two consecutive large-scale TIDs immediately after the beginning of the storm (06:20–08:00 UT). The first TID propagated at 270 m/s with the azimuth of 217°, and the second TID propagated at 500 m/s with the azimuth of 191°. These speeds are close to those used in this work, so it could be the same one that comes traveling from the north, while we have used an azimuth of 180° for the direction of propagation. Also, this agrees with our work in that the disturbance has more than one peak. Finally, this calculation confirms that the source region is in the north. According to Ding et al. (2007), the source of the TIDs was likely located between 50°N and 55°N.

6. Conclusions

We have attempted to reproduce the drastic effects observed at equatorial and low-latitude ionosphere in the Brazilian region (Sao Luis, Fortaleza and Cachoeira Paulista) during the first day (29 October 2003) of the very intense Halloween geomagnetic storms. We have used the SUPIM-INPE model to simulate the $foF2$ and $hmF2$ ionospheric parameters.

Due to the absence of vertical drift measurements in the South American sector during this geomagnetic storm, we have used a new disturbed vertical drift assumed to be the composite of two parts: The first one is the same of disturbed drift derived from IEF and a quiet time well-known equatorial latitude model; the second one is derived from time variation of the F region virtual height. The simulations using this drift are consistent with the observations at the equatorial latitude (Sao Luis and Fortaleza). For low latitude (Cachoeira Paulista), there is a need to introduce a disturbed wind in order to reproduce the observations.

A novel traveling wave-like disturbance propagating from north to south with a 300 m/s velocity is used as a disturbed thermospheric wind which reproduced well the observation in Cachoeira Paulista. This same disturbed wind is found to be appropriate to simulate the ionospheric parameters for Fortaleza and Sao Luis, which are located at the same longitude sector as Cachoeira Paulista.

The proposed disturbed wind model is consistent to explain the published results for TEC in the European region and for $hmF2$ in the North American sector.

References

Abdu, M. A. (2005). Equatorial ionosphere–thermosphere system: Electrodynamics and irregularities. *Advances in Space Research*, *35*(5), 771–787. https://doi.org/10.1016/j.asr.2005.03.150

Abdu, M. A., Souza, J. R., Batista, I. S., Fejer, B. G., & Sobral, J. H. A. (2013). Sporadic layer development and disruption at low latitudes by prompt penetration electric fields during magnetic storms. *Journal of Geophysical Research: Space Physics*, *118*, 2639–2647. https://doi.org/10.1002/jgra.50271

Anderson, D., Anghel, A., Chau, J., & Veliz, O. (2004). Daytime vertical E × B drift velocities inferred from ground-based magnetometer observations at low latitudes. *Space Weather*, *2*, S11001. https://doi.org/10.1029/2004SW000095

Anderson, D., Anghel, A., Chau, J. L., & Yumoto, K. (2006). Global, low-latitude, vertical E × B drift velocities inferred from daytime magnetometer observations. *Space Weather*, *4*, S08003. https://doi.org/10.1029/2005SW000193

Anderson, D., Anghel, A., Yumoto, K., Ishitsuka, M., & Kudeki, E. (2002). Estimating daytime vertical E × B drift velocities in the equatorial F-region using ground-based magnetometer observations. *Geophysical Research Letters*, *29*(12), 1596. https://doi.org/10.1029/2001GL014562

Bailey, G. J., & Balan, N. (1996). A low-latitude ionosphere-plasmasphere model. In R. W. Schunk (Ed.), *Solar-Terrestrial Energy Program: Handbook of Ionospheric Models Center for Atmospheric and Space Sciences* (pp. 173–206). Logan, Utah: Utah State University.

Bailey, G. J., & Sellek, R. (1990). A mathematical model of the Earth's plasmasphere and its application in a study of He at L = 3. *Annales de Geophysique*, *8*(3), 171–189.

Bailey, G. J., Sellek, R., & Rippeth, Y. (1993). A modelling study of the equatorial topside ionosphere. *Annales de Geophysique*, *11*(4), 263–272.

Balan, N., Bailey, G., & Titheridge, J. (1995). Modelling studies of north-south differences in the ionosphere at mid latitudes. *Advances in Space Research*, *16*(5), 99–102. https://doi.org/10.1016/0273-1177(95)00177-g

Balan, N., Otsuka, Y., Nishioka, M., Liu, J. Y., & Bailey, G. J. (2013). Physical mechanisms of the ionospheric storms at equatorial and higher latitudes during the recovery phase of geomagnetic storms. *Journal of Geophysical Research: Space Physics*, *118*, 2660–2669. https://doi.org/10.1002/jgra.50275

Balan, N., Shiokawa, K., Otsuka, Y., Kikuchi, T., Vijaya Lekshmi, D., Kawamura, S., et al. (2010). A physical mechanism of positive ionospheric storms at low latitudes and midlatitudes. *Journal of Geophysical Research*, *115*, A02304. https://doi.org/10.1029/2009JA014515

Balan, N., Shiokawa, K., Otsuka, Y., Watanabe, S., & Bailey, G. J. (2009). Super plasma fountain and equatorial ionization anomaly during penetration electric field. *Journal of Geophysical Research*, *114*, A03310. https://doi.org/10.1029/2008JA013768

Balthazor, R. L., & Moffett, R. J. (1997). A study of atmospheric gravity waves and travelling ionospheric disturbances at equatorial latitudes. *Annales Geophysicae*, *15*(8), 1048–1056. https://doi.org/10.1007/s00585-997-1048-4

Batista, I., Abdu, M., Nogueira, P. A., Paes, R., Souza, J., Reinisch, B., & Rios, V. (2012). Early morning enhancement in ionospheric electron density during intense magnetic storms. *Advances in Space Research*, *49*(11), 1544–1552. https://doi.org/10.1016/j.asr.2012.01.006

Batista, I. S., Abdu, M. A., Souza, J. R., Bertoni, F., Matsuoka, M. T., Camargo, P. O., & Bailey, G. J. (2006). Unusual early morning development of the equatorial anomaly in the Brazilian sector during the Halloween magnetic storm. *Journal of Geophysical Research*, *111*, A05307. https://doi.org/10.1029/2005JA011428

Batista, I. S., Diogo, E. M., Souza, J. R., Abdu, M. A., & Bailey, G. J. (2011). Equatorial ionization anomaly: The role of thermospheric winds and the effects of the geomagnetic field secular variation. In M. A. Abdu, D. Pancheva, & A. Bhattacharyya (Eds.), *Aeronomy of the Earth's Atmosphere and Ionosphere* (1st ed., Vol. 2, pp. 317–328). London: Springer. https://doi.org/10.1007/978-94-007-0326-1_23

Bittencourt, J. A., & Abdu, M. A. (1981). A theoretical comparison between apparent and real vertical ionization drift velocities in the equatorial F region. *Journal of Geophysical Research*, *86*(A4), 2451–2454. https://doi.org/10.1029/JA086iA04p02451

Bittencourt, J. A., Pillat, V. G., Fagundes, P. R., Sahai, Y., & Pimenta, A. A. (2007). LION: A dynamic computer model for the low-latitude ionosphere. *Annales de Geophysique*, *25*, 2371–2392. https://doi.org/10.5194/angeo-25-2371-2007

Blagoveshchensky, D. V., MacDougall, J. W., & Piatkova, A. V. (2006). Ionospheric effects preceding the October 2003 Halloween storm. *Journal of Atmospheric and Solar-Terrestrial Physics*, *68*(7), 821–831. https://doi.org/10.1016/j.jastp.2005.10.017

Blanc, M., & Richmond, A. (1980). The ionospheric disturbance dynamo. *Journal of Geophysical Research*, *85*(A4), 1669–1686. https://doi.org/10.1029/JA085iA04p01669

Borries, C., Jakowski, N., & Wilken, V. (2009). Storm induced large scale TIDs observed in GPS derived TEC. *Annales de Geophysique*, *27*, 1605–1612. https://doi.org/10.5194/angeo-27-1605-2009

Bravo, M. A., Batista, I. S., Souza, J. R., & Foppiano, A. J. (2017). Equatorial ionospheric response to different estimated disturbed electric fields as investigated using Sheffield University Plasmasphere Ionosphere Model at INPE. *Journal of Geophysical Research: Space Physics*, *122*, 10,511–10,527. https://doi.org/10.1002/2017JA024265

Burke, W. J., Gentile, L. C., & Huang, C. Y. (2007). Penetration electric fields driving main phase Dst. *Journal of Geophysical Research*, *112*, A07208. https://doi.org/10.1029/2006JA012137

Chau, J. L., & Woodman, R. F. (2004). Daytime vertical and zonal velocities from 150-km echoes: Their relevance to F-region dynamics. *Geophysical Research Letters*, *31*, L17801. https://doi.org/10.1029/2004GL020800

Chen, X., Lei, J., Wang, W., Burns, A. G., Luan, X., & Dou, X. (2016). A numerical study of nighttime ionospheric variations in the American sector during 28–29 October 2003. *Journal of Geophysical Research: Space Physics*, *121*, 8985–8994. https://doi.org/10.1002/2016JA023091

Denardini, C. M., Aveiro, H. C., Almeida, P. D. S. C., Resende, L. C. A., Guizelli, L. M., Moro, J., et al. (2011). Daytime efficiency and characteristic time scale of interplanetary electric fields penetration to equatorial latitude ionosphere. *Journal of Atmospheric and Solar-Terrestrial Physics*, *73*(11-12), 1555–1559. https://doi.org/10.1016/j.jastp.2010.09.003

Ding, F., Wan, W., Ning, B., & Wang, M. (2007). Large-scale traveling ionospheric disturbances observed by GPS total electron content during the magnetic storm of 29-30 October 2003. *Journal of Geophysical Research*, *112*, A06309. https://doi.org/10.1029/2006JA012013

Fuller-Rowell, T. J., Codrescu, M. V., Moffett, R. J., & Quegan, S. (1994). Response of the thermosphere and ionosphere to geomagnetic storms. *Journal of Geophysical Research*, *99*(A3), 3893–3914. https://doi.org/10.1029/93JA02015

Gouin, P. (1962). Reversal of the magnetic daily variation of Addis-Ababa. *Nature*, *193*(4821), 1145–1146. https://doi.org/10.1038/1931145a0

Hedin, A. E., Fleming, E. L., Manson, A. H., Schmidlin, F. J., Avery, S. K., Clark, R. R., et al. (1996). Empirical wind model for the upper, middle and lower atmosphere. *Journal of Atmospheric and Terrestrial Physics*, *58*(13), 1421–1447. https://doi.org/10.1016/0021-9169(95)00122-0

Huang, C.-S., Rich, R. J., & Burke, W. J. (2010). Storm time electric fields in the equatorial ionosphere observed near the dusk meridian. *Journal of Geophysical Research*, *115*, A08313. https://doi.org/10.1029/2009JA015150

Huang, C.-S., Sazykin, S., Chau, J., Maruyama, N., & Kelley, M. (2007). Penetration electric fields: Efficiency and characteristic time scale. *Journal of Atmospheric and Solar-Terrestrial Physics*, *69*, 1135–1146. https://doi.org/10.1016/j.jastp.2006.08.016

Huba, J. D., Joyce, G., & Fedder, J. A. (2000). Sami2 is Another Model of the Ionosphere (SAMI2): A new low-latitude ionosphere model. *Journal of Geophysical Research*, *105*(A10), 23,035–23,053. https://doi.org/10.1029/2000JA000035

Kelley, M. C. (2009). *The earth's ionosphere: Plasma physics & electrodynamics*. San Diego, CA: Academic Press.

Kelley, M. C., Makela, J. J., Chau, J. L., & Nicolls, M. J. (2003). Penetration of the solar wind electric field into the magnetosphere/ionosphere system. *Geophysical Research Letters*, *30*(4), 1158. https://doi.org/10.1029/2002GL016321

Kelley, M. C., & Retterer, J. (2008). First successful prediction of a convective equatorial ionospheric storm using solar wind parameters. *Space Weather*, *6*, S08003. https://doi.org/10.1029/2007SW000381

Lin, C. H., Richmond, A. D., Heelis, R. A., Bailey, G. J., Lu, G., Liu, J. Y., et al. (2005). Theoretical study of the low- and midlatitude ionospheric electron density enhancement during the October 2003 superstorm: Relative importance of the neutral wind and the electric field. *Journal of Geophysical Research*, *110*, A12312. https://doi.org/10.1029/2005JA011304

Nogueira, P. A. B., Abdu, M. A., Souza, J. R., Bailey, G. J., Batista, I. S., Shume, E. B., & Denardini, C. M. (2013). Longitudinal variation in GNSS -TEC and topside ion density over South American sector associated with the four-peaked wave structures. *Journal of Geophysical Research: Space Physics*, *118*, 7940–7953. https://doi.org/10.1002/2013JA019266

Picone, J. M., Hedin, A. E., Drob, D. P., & Aikin, A. C. (2002). NRLMSISE-00 empirical model of the atmosphere: Statistical comparisons and scientific issues. *Journal of Geophysical Research*, *107*(A12), 1468. https://doi.org/10.1029/2002JA009430

Prolss, G. W. (1977). Seasonal variations of atmospheric-ionospheric disturbances. *Journal of Geophysical Research*, *82*(10), 1635–1640. https://doi.org/10.1029/JA082i010p01635

Prölss, G. W., & Jung, M. J. (1978). Travelling atmospheric disturbances as a possible explanation for daytime positive storm effects of moderate duration at middle latitudes. *Journal of Atmospheric and Terrestrial Physics*, *40*(12), 1351–1354. https://doi.org/10.1016/0021-9169(78)90088-0

Richards, P. G., Fennelly, J. A., & Torr, D. G. (1994). EUVAC: A solar EUV flux model for aeronomic calculations. *Journal of Geophysical Research*, *99*(A5), 8981–8992. https://doi.org/10.1029/94JA00518

Richmond, A. D., & Matsushita, S. (1975). Thermospheric response to a magnetic substorm. *Journal of Geophysical Research*, *80*(19), 2839–2850. https://doi.org/10.1029/JA080i019p02839

Rishbeth, H. (1975). F-region storms and thermospheric circulation. *Journal of Atmospheric and Terrestrial Physics*, *37*, 1055–1064. https://doi.org/10.1016/0021-9169(75)90013-6

Santos, A. M., Abdu, M. A., Souza, J. R., Batista, I. S., & Sobral, J. H. A. (2017). Unusual behavior of quiet-time zonal and vertical plasma drift velocities over Jicamarca during the recent extended solar minimum of 2008. *Annales de Geophysique*, *35*, 1219–1229. https://doi.org/10.5194/angeo-35-1219-2017

Santos, A. M., Abdu, M. A., Souza, J. R., Sobral, J. H. A., & Batista, I. S. (2016). Disturbance zonal and vertical plasma drifts in the Peruvian sector during solar minimum phases. *Journal of Geophysical Research: Space Physics*, *121*, 2503–2521. https://doi.org/10.1002/2015JA022146

Scherliess, L., & Fejer, B. G. (1999). Radar and satellite global equatorial F region vertical drift model. *Journal of Geophysical Research*, *104*(A4), 6829–6842. https://doi.org/10.1029/1999JA900025

Schunk, R. W. (1996). *Solar-terrestrial energy program: Handbook of ionospheric models Center for Atmospheric and Space Sciences*. Logan, Utah: Utah State University.

Shiokawa, K., Lu, G., Otsuka, Y., Ogawa, T., Yamamoto, M., Nishitani, N., & Sato, N. (2007). Ground observation and AMIE-TIEGCM modeling of a storm-time traveling ionospheric disturbance. *Journal of Geophysical Research*, *112*, A05308. https://doi.org/10.1029/2006JA011772

Skoug, R. M., Gosling, J. T., Steinberg, J. T., Mccomas, D. J., Smith, C. W., Ness, N. F., et al. (2004). Extremely high speed solar wind: 29–30 October 2003. *Journal of Geophysical Research*, *109*, A09102. https://doi.org/10.1029/2004JA010494

Souza, J., Brum, C., Abdu, M., Batista, I., Asevedo, W., Bailey, G., & Bittencourt, J. (2010). Parameterized regional ionospheric model and a comparison of its results with experimental data and IRI representations. *Advances in Space Research*, *46*, 1032–1038. https://doi.org/10.1016/j.asr.2009.11.025

Souza, J. R., Asevedo, W. D. Jr., dos Santos, P. C. P., Petry, A., Bailey, G. J., Batista, I. S., & Abdu, M. A. (2013). Longitudinal variation of the equatorial ionosphere: Modeling and experimental results. *Advances in Space Research*, *51*, 654–660. https://doi.org/10.1016/j.asr.2012.01.023

Thampi, S. V., Balan, N., Liu, H., & Yamamoto, M. (2011). Mid-latitude summer nighttime anomaly (MSNA)—Observations and model simulations. *Annales de Geophysique*, *29*, 157–165. https://doi.org/10.5194/angeo-29-157-2011

Tobiska, W., Woods, T., Eparvier, F., Viereck, R., Floyd, L., Bouwer, D., et al. (2000). The SOLAR2000 empirical solar irradiance model and forecast tool. *Journal of Atmospheric and Solar-Terrestrial Physics*, *62*(14), 1233–1250. https://doi.org/10.1016/S1364-6826(00)00070-5

Tsurutani, B., Mannucci, A., Iijima, B., Abdu, M. A., Sobral, J. H. A., Gonzalez, W., et al. (2004). Global dayside ionospheric uplift and enhancement associated with interplanetary electric fields. *Journal of Geophysical Research*, *109*, A08302. https://doi.org/10.1029/2003JA010342

Wei, Y., Hong, M., Wan, W., du, A., Lei, J., Zhao, B., et al. (2008). Unusually long lasting multiple penetration of interplanetary electric field to equatorial ionosphere under oscillating IMF B_Z. *Geophysical Research Letters*, *35*, L02102. https://doi.org/10.1029/2007GL032305